J. Fluid Mech. (2004), *vol.* 513, *pp.* 199–220.
DOI: 10.1017/S0022112004000023 Printed in the United Kingdom

Magnetohydrodynamic turbulence at moderate magnetic Reynolds number

By B. KNAEPEN[1], S. KASSINOS[1,3] AND D. CARATI[2]

[1]Center for Turbulence Research, Stanford University/NASA Ames Research Center, Stanford University, CA 94305-3035, USA

[2]Universté Libre de Bruxelles, Statistical and Plasma Physics, CP231, Boulevard du Triomphe, Campus Plaine, 1050 Brussels, Belgium

[3]Department of Mechanical and Manufacturing Engineering, University of Cyprus, 75 Kallipoleos, Nicosia 1678, Cyprus

(Received 15 May 2003 and in revised form 13 April 2004)

We consider the case of homogeneous turbulence in a conducting fluid that is exposed to a uniform external magnetic field at low to moderate magnetic Reynolds numbers (by moderate we mean here values as high as 20). When the magnetic Reynolds number is vanishingly small ($R_m \ll 1$), it is customary to simplify the governing magnetohydrodynamic (MHD) equations using what is known as the quasi-static (QS) approximation. As the magnetic Reynolds number is increased, a progressive transition between the physics described by the QS approximation and the MHD equations occurs. We show here that this intermediate regime can be described by another approximation which we call the quasi-linear (QL) approximation. For the numerical simulations performed, the predictions of the QL approximation are in good agreement with those of MHD for magnetic Reynolds number up to $R_m \sim 20$.

1. Introduction

1.1. *Motivation and objectives*

Magnetohydrodynamics (MHD) applies to many conductive fluid and plasma flows encountered in nature and in industrial applications. In numerous circumstances, the flow is subject to a strong mean magnetic field. This happens in the earth's liquid core and is ubiquitous in solar physics for topics such as sunspots, solar flares, solar corona, solar wind, etc. Mean magnetic fields play an important role on even larger scales, for instance in the dynamics of the interstellar medium. Among the industrial applications involving applied external magnetic fields are drag reduction in duct flows, design of efficient coolant blankets in tokamak fusion reactors, control of turbulence of immersed jets in the steel casting process and advanced propulsion and flow control schemes for hypersonic vehicles.

Depending on the application, the magnetic Reynolds number, R_m, can vary tremendously. In astrophysical problems, R_m can be extremely high as a result of the dimensions of the objects studied. On the contrary, for most industrial flows involving liquid metal, R_m is very low, usually less than 10^{-2}. When an external magnetic field is present, it is customary at such low values of R_m to make use of the so-called quasi-static (QS) approximation. In this approximation, induced magnetic fluctuations are much smaller than the applied magnetic field and the overall magnetic effect amounts to adding in the Navier–Stokes equations an extra damping term which

only affects Fourier modes having a component parallel to the magnetic field (more details below). The derivation of the QS approximation involves taking the limit of vanishing R_m and its domain of validity is thus an interesting question. Indeed certain applications, such as advanced schemes for the control of magnetogasdynamic flows around hypersonic vehicles, involve values of R_m of the order 1 to 10 (see e.g. Poggie & Gaitonde 2002). It is thus valuable to possess reliable approximations in this regime that can be used in place of the full nonlinear MHD (in the sequel, when referring to MHD, we always mean the full nonlinear theory).

The limit of vanishing R_m (with mean magnetic field) has been the subject of several theoretical studies in the past. Lehnert (1955) concentrates on the final period of decay of a convective fluid governed by the completely linearized MHD equations ($Re \ll 1, \ R_m \ll 1$). The suppression of turbulence by a magnetic field was studied in Moffatt (1967) ($Re \gg 1, \ R_m \ll 1$) again using linearized equations. In short, both works focus on the time evolution of the energy of the Fourier modes as a function of their wave vectors. Using prescribed energy spectra, Moffatt (1967) also obtains global energy decay rates. In another theoretical investigation relevant to the present study Davidson (1995) derives in the quasi-static framework the conservation of momentum and angular momentum parallel to the direction of the magnetic field (neglecting viscous dissipation). Focusing on jets and vortices, the author then describes how the flow structures need to elongate in the direction of the magnetic field in order to lower their energy loss while satisfying the above conservation laws. The elongation of structures in the direction of the magnetic field was also studied earlier in Sommeria & Moreau (1982), however, in the context of linearized equations.

To our knowledge, the first numerical study of MHD turbulence in the regime $R_m \ll 1$ is due to Schumann (1976). All the simulations in that work were done using a modified three-dimensional spectral code implementing the QS approximation. However, because of the computer resources available at that time, the resolution of the simulations was limited to 32^3 grid points. The numerical experiment of Schumann (1976) reproduces the thought experiment described in Moffatt (1967) in which an initially homogeneous isotropic flow is suddenly subjected to an applied external magnetic field. A quantitative description of the magnetic damping and building of anisotropy is presented as well as the dependence of the results on the presence or not of the nonlinear term in the Navier–Stokes equation. Again considering the QS approximation, the case of forced turbulence in a three-dimensional periodic domain has first been studied in Hossain (1991) and more recently in Zikanov & Thess (1998).

Performing MHD simulations in the limit of low R_m is impractical. Aside from the increased complexity arising from having to carry a separate evolution equation for the magnetic field, the main problem lies in the time scales involved in the problem. Indeed, at vanishing magnetic Reynolds number, the magnetic diffusion time scale tends to zero. The only possibility in that case is to resort to the QS approximation for which this time scale is not explicitly relevant. Simulations of MHD have thus been restricted so far to cases where the magnetic and kinetic time scales are of the same order. This is the case when the magnetic Prandtl number (see below) is close to 1. Among the numerous previous numerical studies of MHD in this regime, we mention the work of Oughton, Priest & Matthaeus (1994) which is the most relevant to the present discussion. They consider the same three-dimensional periodic geometry with an applied external magnetic field as in Schumann (1976).

In the present article, we will consider the decay of MHD turbulence under the influence of a strong external magnetic field at moderate magnetic Reynolds numbers. Typical values of R_m that are considered here range from ~ 0.1 to ~ 20. As

Resolution	256^3
Box size ($l_x \times l_y \times l_z$)	$2\pi \times 2\pi \times 2\pi$
Rms velocity	1.76
Viscosity	0.006
Integral length-scale ($3\pi/4 \times (\int \kappa^{-1} E(\kappa)\,\mathrm{d}\kappa \int E(\kappa)\,\mathrm{d}\kappa)$)	0.679
$Re = uL/\nu$	199
Dissipation (ϵ)	8.39
Dissipation scale ($\gamma = (\nu^3/\epsilon)^{1/4}$))	0.0127
$k_{max}\gamma$	1.62
Microscale Reynolds number ($R_\lambda = \sqrt{15/(\nu\epsilon)}u^2$)	53.5
Eddy turnover time ($\tau = (3/2)u/\epsilon$))	0.554

TABLE 1. Turbulence characteristics of the initial velocity field. All quantities are in m.k.s. units.

a comparison, the initial kinetic Reynolds number common to all our simulations is $Re_L = 199$. This means that the range of Prandtl numbers explored is 5×10^{-4} to 10^{-1}. Our motivation is mainly to exhibit how the transition from the QS approximation to MHD occurs. At the lowest values of R_m studied here, the QS approximation is shown to model the flow faithfully. However, for the higher values of R_m considered, it is clearly inadequate but can be replaced by another approximation which will be referred to as the quasi-linear (QL) approximation. Another objective of the present study is to describe how variations in the magnetic Reynolds number (while maintaining all other parameters constant) affect the dynamics of the flow. This complements past studies where variations in either the strength of the external magnetic field or the kinetic Reynolds number were considered.

This article is organized as follows. In § 2, we review the derivation of the quasi-static approximation and stress the assumptions that might pose a problem as the magnetic Reynolds number is increased. Section 3 is devoted to the description of the numerical experiments performed using the quasi-static approximation and MHD. In § 4, we describe the quasi-linear approximation and test it numerically against full MHD. A concluding summary is given in § 5.

2. MHD equations in the presence of a mean magnetic field

2.1. *Dimensionless parameters*

Two dimensionless parameters are usually introduced to characterize the effects of a uniform magnetic field applied to unstrained homogeneous turbulence in an electrically conductive fluid. They are the magnetic Reynolds number R_m and the interaction number N (also known as the Stuart number):

$$R_m \equiv \frac{vL}{\eta} = \left(\frac{L^2}{\eta}\right)\Big/\left(\frac{L}{v}\right), \quad N \equiv \frac{\sigma B^2 L}{\rho v} = \frac{\tau}{\tau_m}. \tag{2.1}$$

In the above expressions, $v = \sqrt{\langle u_i u_i \rangle /3}$ is the r.m.s. of the fluctuating velocity u_i; L is the integral length scale of the flow (defined in table 1); $\eta = 1/(\sigma\mu)$ is the magnetic diffusivity where σ is the electric conductivity of the fluid, and μ is the fluid magnetic permeability; ρ is the fluid density and B is the strength of the applied external magnetic field. The magnetic Reynolds number represents the ratio of the characteristic time scale for diffusion of the magnetic field L^2/η to the time scale of the turbulence $\tau = L/v$. Related to R_m, we can also define a magnetic Prandtl number

representing the ratio of R_m to the hydrodynamic Reynolds number Re_L,

$$P_m \equiv \frac{\nu}{\eta} = \frac{R_m}{Re_L}, \qquad Re_L = \frac{vL}{\nu}. \tag{2.2}$$

The interaction number N represents the ratio of the large-eddy turnover time τ to the Joule time $\tau_m = \rho/(\sigma B^2)$, i.e. the characteristic time scale for dissipation of turbulent kinetic energy by the action of the Lorentz force (see e.g. Davidson 2001). N can be viewed as a measure of the ability of an imposed magnetic field to drive the turbulence to a two-dimensional three-component state. Indeed, under the continuous action of the Lorentz force, energy becomes increasingly concentrated in modes independent of the coordinate direction aligned with $\boldsymbol{B}$. As a two-dimensional state is approached, Joule dissipation decreases because fewer and fewer modes with gradients in the direction of $\boldsymbol{B}$ are left available. In addition, the tendency towards two-dimensionality and anisotropy is continuously opposed by nonlinear angular energy transfer from modes perpendicular to $\boldsymbol{B}$ to other modes, which tends to restore isotropy. If N is larger than some critical value N_c, the Lorentz force is able to drive the turbulence to a state of complete two-dimensionality. For smaller N, the Joule dissipation is balanced by nonlinear transfer before complete two-dimensionality is reached. For very small N, the anisotropy induced by the Joule dissipation is negligible.

2.2. *The quasi-static approximation*

In this section, we review the derivation of the quasi-static approximation (Roberts 1967). Although standard, the inclusion of the discussion here will prove useful when introducing the quasi-linear approximation in § 4.

If the external magnetic field B_i^{ext} is explicitly separated from the fluctuations b_i, the incompressible MHD equations can be written as

$$\partial_t u_i = -\partial_i(p/\rho) - u_j\partial_j u_i + \frac{1}{(\mu\rho)}\left(B_j^{ext} + b_j\right)\partial_j\left(B_i^{ext} + b_i\right) + \nu\Delta u_i, \tag{2.3}$$

$$\partial_t\left(B_i^{ext} + b_i\right) = -u_j\partial_j\left(B_i^{ext} + b_i\right) + \left(B_j^{ext} + b_j\right)\partial_j u_i + \eta\Delta\left(B_i^{ext} + b_i\right), \tag{2.4}$$

where p is the sum of the kinematic and magnetic pressures and ν is the kinematic viscosity. Since we consider initially isotropic freely decaying homogeneous turbulence, there is no mean velocity field. Therefore, for the sake of simplicity, we avoid introducing explicitly a decomposition of the velocity field into mean and fluctuating parts. Also, the external magnetic field is taken to be homogeneous and stationary so that (2.3) and (2.4) reduce to

$$\partial_t u_i = -\partial_i(p/\rho) - u_j\partial_j u_i + \frac{1}{(\mu\rho)}b_j\partial_j b_i + \frac{1}{(\mu\rho)}B_j^{ext}\partial_j b_i + \nu\Delta u_i, \tag{2.5}$$

$$\partial_t b_i = -u_j\partial_j b_i + b_j\partial_j u_i + B_j^{ext}\partial_j u_i + \eta\Delta b_i. \tag{2.6}$$

As pointed out in Roberts (1967), (2.6) can be simplified considerably for flows at low magnetic Reynolds numbers. Indeed, by definition, the limit $R_m \ll 1$ describes flows for which nonlinear terms resulting from magnetic fluctuations are negligible when compared to the dissipative term in (2.6). This is easily seen by adopting the traditional scalings,

$$\|u_j\partial_j b_i\| = \frac{vb}{L}, \quad \|b_j\partial_j u_i\| = \frac{vb}{L}, \quad \|\eta\Delta b_i\| = \frac{\eta b}{L^2}, \tag{2.7}$$

where $b = \sqrt{\overline{b_i b_i}/3}$, and noting that

$$R_m = \frac{vL}{\eta} = \frac{\|u_j \partial_j b_i\|}{\|\eta \Delta b_i\|} = \frac{\|b_j \partial_j u_i\|}{\|\eta \Delta b_i\|}. \tag{2.8}$$

In place of (2.6) we thus have, in the limit $R_m \ll 1$,

$$\partial_t b_i = B_j^{ext} \partial_j u_i + \eta \Delta b_i. \tag{2.9}$$

The so-called quasi-static (QS) approximation is obtained by further assuming that $\partial_t b_i \approx 0$ in (2.9). To understand how this comes about, we consider the time scales of the two terms on the right-hand side of (2.9). Since B^{ext} is independent of time, the time scale of $B_j^{ext} \partial_j u_i$ is $\mathscr{T} = L/v$, while the time scale of the diffusion term can be identified with the damping time $\mathscr{T}^* = L^2/\eta$. The ratio of these two time scales is then

$$\frac{\mathscr{T}^*}{\mathscr{T}} = R_m, \tag{2.10}$$

indicating that at low magnetic Reynolds number, diffusion time is much smaller than large-eddy turnover time. This justifies the assumption $\partial_t b_i \approx 0$ since the magnetic fluctuations then adapt instantaneously to the slowly varying velocity field and reach their asymptotic values for which $\partial_t b_i \approx 0$ (see §4 for more details). In the QS approximation, we thus have

$$\eta \Delta b_i = -B_j^{ext} \partial_j u_i. \tag{2.11}$$

Using a Fourier representation for u_i and b_i, this equation is readily solved and yields

$$b_m(\boldsymbol{k}, t) = \mathrm{i} \frac{(B_j^{ext} k_j)}{\eta k^2} u_m(\boldsymbol{k}, t), \tag{2.12}$$

where we have defined

$$u_m(\boldsymbol{k}, t) = \sum_{\boldsymbol{x}} u_m(\boldsymbol{x}, t) \exp(-\mathrm{i}\boldsymbol{k} \cdot \boldsymbol{x}), \quad b_m(\boldsymbol{k}, t) = \sum_{\boldsymbol{x}} b_m(\boldsymbol{x}, t) \exp(-\mathrm{i}\boldsymbol{k} \cdot \boldsymbol{x}). \tag{2.13}$$

Since b_i is now expressed completely in terms of u_i, the evolution equation for the velocity field can be explicitly closed. In Fourier representation we obtain,

$$\partial_t u_m(\boldsymbol{k}, t) = -\mathrm{i} k_m p'(\boldsymbol{k}, t) - [u_j \partial_j u_i]_m(\boldsymbol{k}, t) - \sigma \frac{(\boldsymbol{B}^{ext} \cdot \boldsymbol{k})^2}{\rho k^2} u_m(\boldsymbol{k}, t) - \nu k^2 u_m(\boldsymbol{k}, t), \tag{2.14}$$

where $p' = p/\rho$ (consistently with the small magnetic fluctuations assumption, the second-order term $b_j \partial_j b_i$ does not appear in (2.14)).

To summarize, two simplifications are required in order to reach (2.14). The first consists in neglecting the nonlinear terms $u_j \partial_j b_i$ and $b_j \partial_j u_i$ in (2.6). The second is obtained by discarding the time derivative of b_i in (2.9). These two simplifications are consequences of the assumption $R_m \ll 1$ and we should thus expect them to break down when the magnetic Reynolds number is increased. In the next sections, we test the QS approximation by comparing its predictions to those obtained using the MHD equations (2.5) and (2.6).

Run number	η	B_A^{ext}	$N(t_0)$	$R_m(t_0)$
1	11.95	5.57	1	0.1
2	1.195	1.76	1	1
3	0.239	0.787	1	5.0
4	0.119	0.557	1	10.0
5	0.0597	0.394	1	20.0
6	11.95	17.6	10	0.1
7	1.195	5.57	10	1
8	0.239	2.49	10	5.0
9	0.119	1.76	10	10.0
10	0.0597	1.24	10	20.0

TABLE 2. Summary of the parameters for the different runs performed.

3. Numerical results: QS vs. MHD

3.1. *Parameters*

To test the domain of validity of the QS approximation, we have used two different pseudospectral codes. The first one simulates the MHD equations (2.5) and (2.6), while the second one simulates (2.14). All the runs presented here have a resolution of 256^3 Fourier modes in a $(2\pi)^3$ computational domain.

The initial condition for the velocity field is common to both codes. It consists of a developed turbulence field that is adequately resolved in the computational domain adopted. Some of its characteristics are given in table 1. For the MHD case, an initial condition for b_i has to be chosen at $t = t_0$. Here, we have made the choice $b_i(t_0) = 0$. In other words, our simulations describe the response of an initially non-magnetized turbulent conductive fluid to the application of a strong magnetic field. The corresponding completely linearized problem has been described in detail in Moffatt (1967). For the QS approximation case, an initial condition for b_i is, of course, not required since the equation for the velocity field is completely closed. In that case, the initial condition for the magnetic field is, in fact, implicitly given by (2.12) at $t = t_0$. We could then argue that the two codes do not simulate the same flow since they do not have the same initial condition for the magnetic field. However, the independence of the QS approximation on the initial magnetic field is an aspect that is interesting to test. If the flow behaves according to the QS approximation, the magnetic field (using MHD) should very rapidly converge to the value given by (2.12).

In order to distinguish between our numerical runs, we will vary the values of the interaction parameter and the magnetic Reynolds number (at $t = t_0$). When these two quantities are set, the only free parameters in the evolution equations (2.5), (2.6) and (2.14) are completely determined, i.e.

$$B_A^{ext} = \frac{N v^2}{R_m}, \quad \eta = \frac{vL}{R_m} \tag{3.1}$$

where B_A^{ext} is the external magnetic field strength in Alfvén units $B_A^{ext} = B^{ext}/\sqrt{\mu\rho}$ and the values of v and L are given in table 1. The values of R_m and N for all our runs are given in table 2 along with the corresponding values of η and B_A^{ext}. Because of the finite computer resources available, we note the following two restrictions about the present work. First, because of the limitation in the achievable kinetic Reynolds number, the simulations (except in the quasi-static limit) do not reach values of the

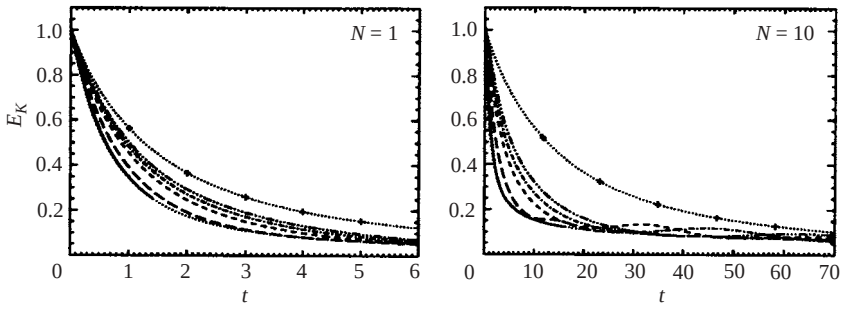

FIGURE 1. Evolution with time of the kinetic energy at different Stuart numbers and magnetic Reynolds numbers. ·····, QS approximation; ———, $R_m = 0.1$; – – –, 1; - - -, 5; – · –, 10; – · · · –, 20; · · · + · · ·, $B^{ext} = 0$.

Prandtl number as low as we could wish and present in traditional liquid–metal applications. Secondly, at the later stage of the kinetic energy decay, flow structures tend to be elongated strongly in the direction of the imposed magnetic field. In that case, the appropriateness of the periodic boundary conditions is questionable. This issue is unavoidable, but thankfully arises only in one direction.

3.2. *Results*

In this section we present some results obtained by performing the simulations detailed in § 3.1.

3.2.1. *Kinetic energy decay*

In figure 1, we plot the time evolution of the normalized kinetic energy,

$$E_K = \frac{1}{E_K(0)} \int \mathrm{d}\boldsymbol{x} \tfrac{1}{2} u_i(\boldsymbol{x}) u_i(\boldsymbol{x}). \tag{3.2}$$

In this and subsequent figures, time has been non-dimensionalized using the Joule timescale (see (2.10)). Keeping N constant, it is clear from the figure that as the magnetic Reynolds number is decreased, the decays converge to the quasi-static limit (dotted curve). At $R_m = 0.1$, MHD and the QS approximation are barely distinguishable for the cases run; at $R_m = 1$, differences are clearly observed. As expected, the discrepancy between MHD and the QS approximation is quite severe at intermediate values of the R_m. We also note here the presence of oscillations in the kinetic energy at long times for the case $N = 10$. Their origin is well known (see e.g. Lehnert 1955 or Moffatt 1967) and results from the laminarization of the flow for long times. In that case, the MHD equations (2.6) and (2.5) reduce to their linear versions and become (in Fourier space) a system of linear oscillators coupled through the external magnetic field. In that limit, turbulence is dominated by the propagation of interacting Alfvén waves. In both figures, the case $B^{ext} = 0$ (i.e. pure hydrodynamics) has been included to emphasize the role of the magnetic field in the other runs.

3.2.2. *Magnetic energy evolution*

The next diagnostic we examine is the evolution of the energy contained in the magnetic fluctuations. This quantity is defined through,

$$E_M = \int \mathrm{d}\boldsymbol{k} \tfrac{1}{2} |b_i(\boldsymbol{k}, t)|^2. \tag{3.3}$$

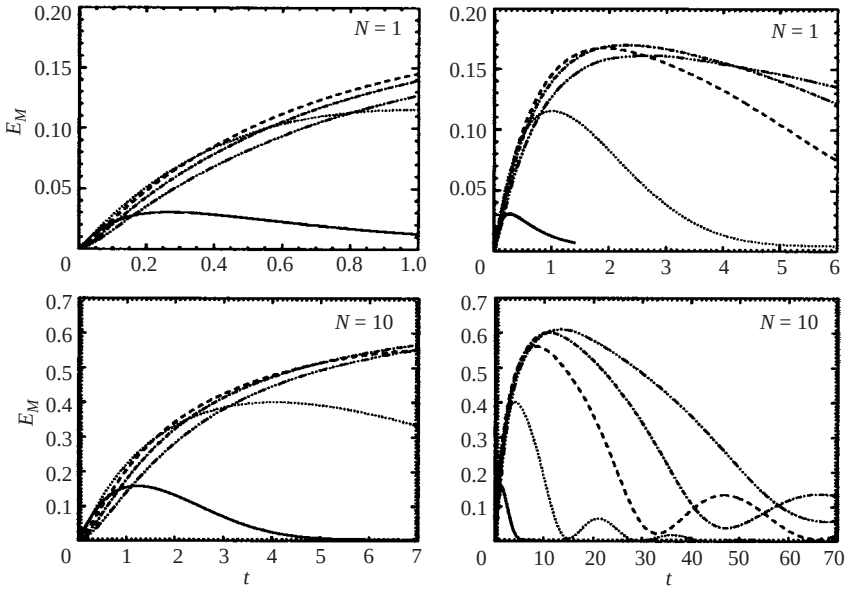

FIGURE 2. Evolution with time of the magnetic energy computed from (3.3). ——, $R_m = 0.1$; – – –, 1; - - -, 5; –·–, 10; –···–, 20.

For each set of runs at fixed N two graphs are presented. The left-hand side graphs represent 'zoomed' versions of the right-hand side graphs and have been included in order to show with more detail the initial magnetic growths for the different runs. At $t = t_0$, the evolution of the magnetic field is determined by,

$$\partial_t b_{i\,|t=0} = B_j^{ext} \partial_j u_{i\,|t=0}\,, \tag{3.4}$$

with B^{ext} given by (3.1). As the magnetic Reynolds number is decreased, the initial slope of (3.3) should thus increase and this is exactly what is observed in the left-hand side graphs of figure 2. After some time, the magnetic energies all reach their maximum value and then start to decrease. The rate of decay increases at lower magnetic Reynolds numbers since in the limit chosen, $\eta = vL/R_m$. Related to the oscillations in the kinetic energy we observe for $N = 10$ some oscillations in the magnetic energy at long times.

In order to describe the transition from QS behaviour to MHD in the simulations as the magnetic Reynolds is increased, a second measure of the magnetic energy can be introduced:

$$E_{M1} = \frac{1}{E_{M1}(t_0)} \int \mathrm{d}\boldsymbol{k} \tfrac{1}{2} \frac{\left(B_j^{ext} k_j\right)^2}{\eta^2 k^4} |u_i(\boldsymbol{k}, t)|^2. \tag{3.5}$$

This is the (normalized) energy of the magnetic fluctuations when they are computed from the QS expression (2.12). When the dynamics are governed by the QS approximation, (3.5) should coincide with $E_M/E_{M1}(t_0)$. This is illustrated in figure 3. At magnetic Reynolds number $R_m = 0.1$, $E_M/E_{M1}(t_0)$ and E_{M1} are very close soon after the external magnetic field is switched on. This indicates that, in a very short time, the magnetic fluctuations forget their initial state and 'align' with the predictions of the QS approximation (2.12). This is entirely in the spirit of the assumption that at low magnetic Reynolds number the time derivative in (2.9) can be neglected (or rather that it is significant only during a very short transient time). At higher values

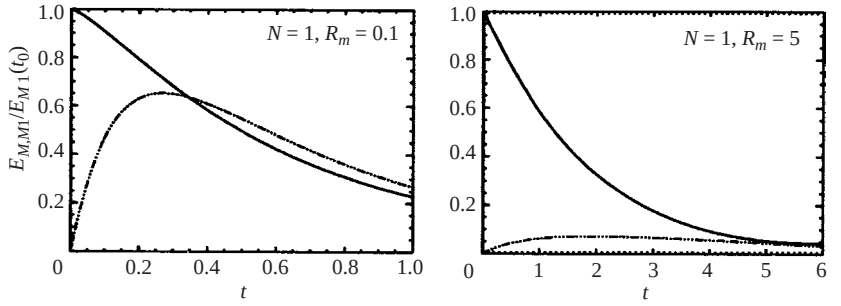

FIGURE 3. Comparison of magnetic energies computed from (3.3) —·—·— and (3.5) ———.

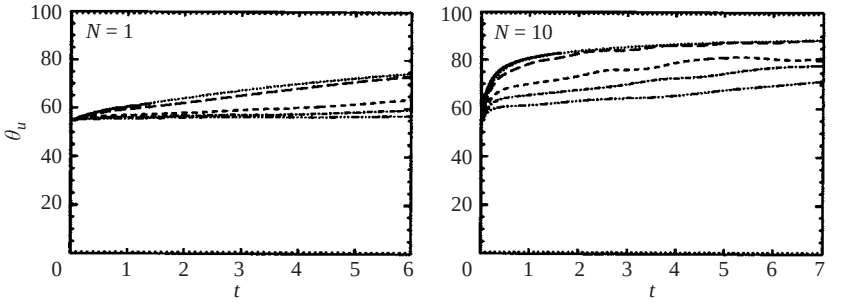

FIGURE 4. Anisotropy angle θ_u computed from (3.6). ·····, QS approximation; ———, $R_m = 0.1$; — — —, 1; - - -, 5; —·—, 10; —·—·—, 20.

of the magnetic Reynolds number, such as $R_m = 5$, this transient time becomes longer and the 'true' energy content of the fluctuations reaches values comparable to those predicted by the QS expression only after several Joule times.

As we expect, this discussion indicates that neglecting the time derivative of b_i in the induction equation is problematic when the magnetic Reynolds number reaches moderate values.

3.2.3. *Anisotropy*

A characteristic feature of MHD flows subject to a strong external magnetic field is the appearance of a strong anisotropy in the flow. In the QS approximation this is easily seen by observing that in (2.14) only Fourier modes with wave vectors having a non-zero projection onto B_i^{ext} are affected by the extra Joule damping. In order to quantify the anisotropy we follow the approach of Shebalin, Matthaeus & Montgomery (1983) and Oughton *et al.* (1994) by introducing the anisotropy angles,

$$\tan^2\theta_u = \frac{\sum k_\perp^2 \|u_i(\boldsymbol{k})\|^2}{\sum k_z^2 \|u_i(\boldsymbol{k})\|^2}, \tag{3.6}$$

$$\tan^2\theta_b = \frac{\sum k_\perp^2 \|b_i(\boldsymbol{k})\|^2}{\sum k_z^2 \|b_i(\boldsymbol{k})\|^2}, \tag{3.7}$$

where $k_\perp = k_x^2 + k_y^2$ and the summations are extended to all values of $\boldsymbol{k}$.

When the flow is completely isotropic, we have $\tan^2\theta_u = 2$ implying $\theta_u \simeq 54.7°$. If the flow becomes independent of the z-direction then $\tan^2\theta_u \to \infty$ or equivalently $\theta_u \to 90°$. Figure 4 shows the evolution with time of θ_u for the different runs. At

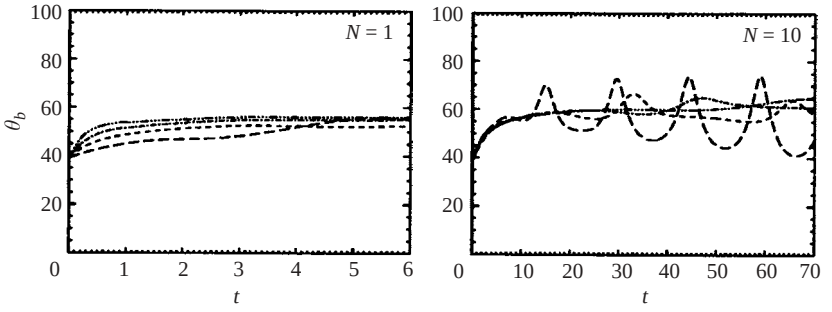

FIGURE 5. Anisotropy angle θ_b computed from (3.7). ·····, QS approximation; $R_m =$ ———, 0.1; – – –, 1; - - -, 5; –·–, 10; —·····—, 20.

$N = 1$, the anisotropy is only important for the QS, $R_m = 0.1$ and $R_m = 1$ runs. For $N = 10$, all the runs become highly anisotropic.

The initial anisotropy in the magnetic field can also be computed exactly. At time $t_0 + \Delta t$ ($\Delta t \ll 1$), $b_i(\boldsymbol{k})$ is computed using (3.4): $b_i(\boldsymbol{k}, t_0 + \Delta t) = \mathrm{i} B_z^{ext} k_z u_i(\boldsymbol{k}, t_0) \Delta t$. This means that at $t_0 + \Delta t$, (3.7) can be rewritten as:

$$\tan^2 \theta_b = \frac{A_x + A_y}{A_z}, \tag{3.8}$$

with

$$A_x = \int \mathrm{d}k_x \mathrm{d}k_y \mathrm{d}k_z \; k_x^2 \; k_z^2 Q(k), \tag{3.9}$$

$$A_y = \int \mathrm{d}k_x \mathrm{d}k_y \mathrm{d}k_z \; k_y^2 \; k_z^2 Q(k), \tag{3.10}$$

$$A_z = \int \mathrm{d}k_x \mathrm{d}k_y \mathrm{d}k_z \; k_z^4 Q(k), \tag{3.11}$$

where $Q(k) = \|u_i(\boldsymbol{k}, t_0)\|^2$ depends only on the norm of $\boldsymbol{k}$ (note that for calculus purposes we have replaced summations by integrals). Switching to spherical coordinates ($k_z = k \cos\theta$, $k_x = k \sin\theta \cos\phi$, $k_y = k \sin\theta \sin\phi$), we observe that the only difference between A_x, A_y and A_z comes from the angular integrations: $A_x = I a_x$, $A_y = I a_y$, $A_z = I a_z$ where,

$$I = \int_0^\infty \mathrm{d}k \; k^6 \; Q(k), \tag{3.12}$$

$$a_x = \int_0^{2\pi} \mathrm{d}\phi \int_0^\pi \mathrm{d}\theta \sin^3\theta \cos^2\phi \cos^2\theta, \tag{3.13}$$

$$a_y = \int_0^{2\pi} \mathrm{d}\phi \int_0^\pi \mathrm{d}\theta \sin^3\theta \sin^2\phi \cos^2\theta, \tag{3.14}$$

$$a_z = \int_0^{2\pi} \mathrm{d}\phi \int_0^\pi \mathrm{d}\theta \sin\theta \cos^4\theta. \tag{3.15}$$

All these angular integrals are easily computed: $a_x = a_y = 4\pi/15$, $a_z = 4\pi/5$. We thus have,

$$\tan^2 \theta_b(t_0 + \Delta t) = \tfrac{2}{3}, \quad \text{i.e.} \quad \theta_b(t_0 + \Delta t) \simeq 39.2^\circ. \tag{3.16}$$

Figure 5 shows the evolution with time of θ_b for the different runs. Both plots exhibit surprising behaviour. In the case $N = 1$, we would expect θ_b to remain close

to its initial value since the velocity field remains largely isotropic (as it is at the beginning of the simulation). Instead, θ_b evolves to a value compatible with an isotropic magnetic field. In the case $N = 10$, some strong oscillations in the magnetic anisotropy are observed. For the times considered, no clear trends in the mean are present. Note that some oscillations are also present in the velocity anisotropy, but are much less pronounced.

4. The quasi-linear approximation

4.1. *Governing equations*

The preceding section indicates that, for our numerical simulations at magnetic Reynolds numbers of the order $10^{-1} - 1$, the QS approximation and MHD produce nearly identical results. For higher values of R_m, the QS approximation is not valid and has to be replaced to predict the flow accurately. Since magnetic fluctuations remain small in all the runs performed, it is natural still to consider a linearized induction equation. However, results reported in § 3.2.2 support the idea that neglecting the time derivative of b_i in the induction equation is not appropriate in the context of moderate R_m.

We thus consider here an intermediate approximation which is defined by the following simplified MHD equations:

$$\partial_t u_i = -\partial_i (p/\rho) - u_j \partial_j u_i + \frac{1}{(\mu\rho)} B_j^{ext} \partial_j b_i + \nu \Delta u_i, \tag{4.1}$$

$$\partial_t b_i = B_j^{ext} \partial_j u_i + \eta \Delta b_i. \tag{4.2}$$

This approximation will be referred to as the quasi-linear (QL) approximation since only the nonlinear terms involving the magnetic field are discarded whereas the nonlinear convective term in the velocity equation is retained. Of course, if $\partial_t b_i$ is neglected in (4.2) we immediately recover the quasi-static approximation.

Equation (4.2) is nothing other than a diffusion equation for the magnetic field with a source term given by $B_j^{ext} \partial_j u_i$. In Fourier space, the solution of this equation is easily obtained and reads,

$$b_i(\boldsymbol{k}, t) = b_i(\boldsymbol{k}, t_0) \exp(-\eta k^2 t) + \mathrm{i} \int_{t_0}^{t} \mathrm{d}\tau k_j B_j^{ext} u_i(\boldsymbol{k}, \tau) \exp(-\eta k^2 (t - \tau)). \tag{4.3}$$

From the first term on the right-hand side of (4.3), we see that the initial condition for b_i is damped more rapidly with increasing magnetic diffusivity (if v and L are constant this is equivalent to a decrease in the magnetic Reynolds number). Note that with the initial condition we have chosen for the magnetic field, i.e. $b_i(t_0) = 0$, this first term vanishes. At high magnetic diffusivity, the integral in (4.3) converges to (2.12) and the QS approximation holds. More explicitly, we have the situation depicted in figure 6. The interval between the dashed lines represents the support in which $\exp(-\eta k^2 (t - \tau))$ is significant and thus where there is some contribution to the integral of (4.3). As η increases, this interval becomes smaller, and $u_i(\boldsymbol{k}, t)$ may be assumed constant in that short period of time. The integration is then immediate and we obtain,

$$b_i(\boldsymbol{k}, t) = b_i(\boldsymbol{k}, 0) \exp(-\eta k^2 t) + \frac{\mathrm{i} k_j B_j^{ext}}{\eta k^2} [1 - \exp(-\eta k^2 (t - t_0))] u_i(\boldsymbol{k}, t), \tag{4.4}$$

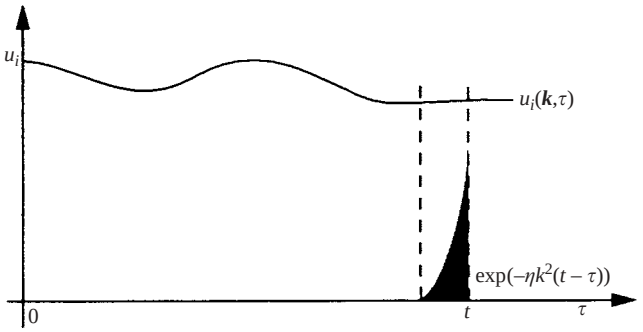

FIGURE 6. Evaluation of $b_i(\boldsymbol{k}, t)$ in the quasi-linear approximation.

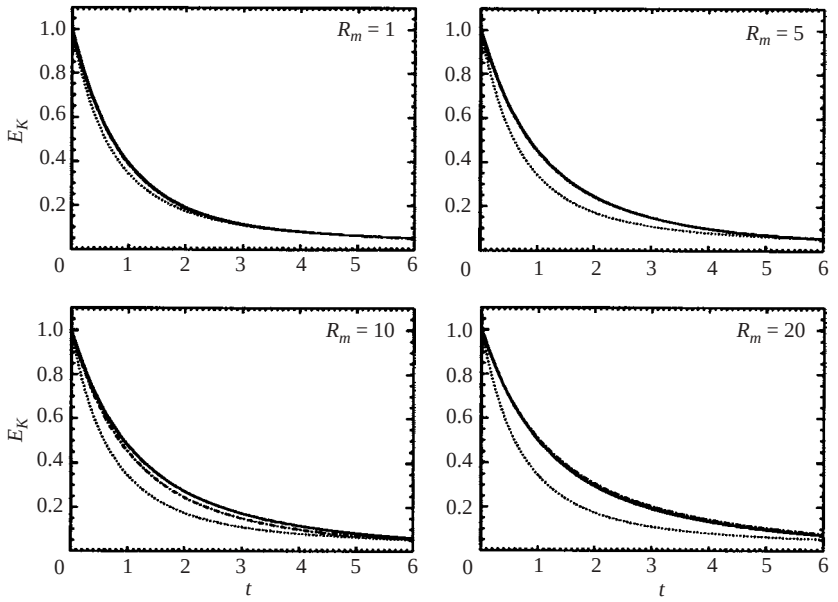

FIGURE 7. Evolution with time of the kinetic energy ($N = 1$). ———, MHD; – · –, QL approximation; ·····, QS approximation.

which converges to (2.12) in the limit $\eta \to \infty$. Thus, the time history of $u_i(\boldsymbol{k}, t)$ plays a role only when η is relatively small, in which case the exponential has a wider support.

4.2. *Results*

In order to compare the QL approximation with MHD, we have performed the same numerical simulations as described in § 3, but this time using (4.1) and (4.2) instead of the QS approximation.

4.2.1. *Kinetic energy decay*

In figures 7 and 8, we present the time history of the kinetic energy (as defined by (3.2)) obtained from both MHD and the QL approximation. For reference, we have also included the predictions obtained using the QS approximation. For $N = 1$, the QL approximation and MHD agree nearly perfectly for all values of the magnetic Reynolds number. For $N = 10$, the agreement is still very good.

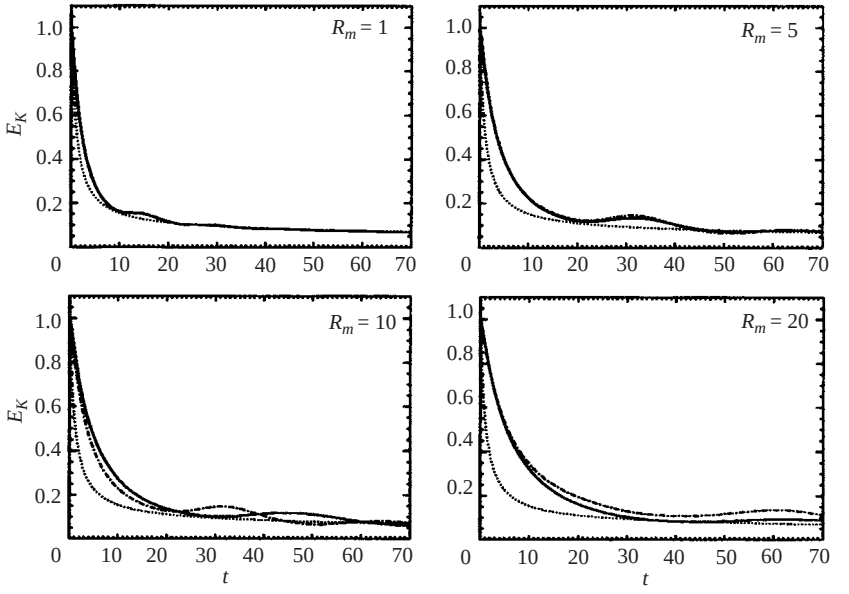

FIGURE 8. Evolution with time of the kinetic energy ($N = 10$). ———, MHD; – · –, QL approximation; ·····, QS approximation.

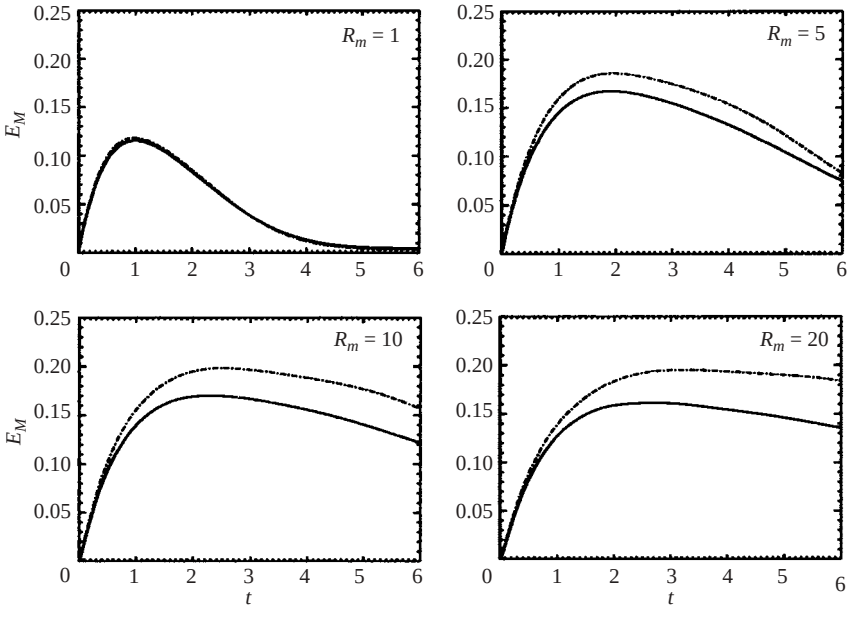

FIGURE 9. Evolution with time of the magnetic energy ($N = 1$). ———, MHD; – · –, QL approximation.

4.2.2. *Magnetic energy evolution*

Figures 9 and 10 represent the time evolution of the energy of the magnetic fluctuations (defined by (3.3)) for the different runs. In all cases, there is a systematic overestimate of the peak energies by the QL approximation. This overestimate is more pronounced for the case at $N = 1$ than for those at $N = 10$.

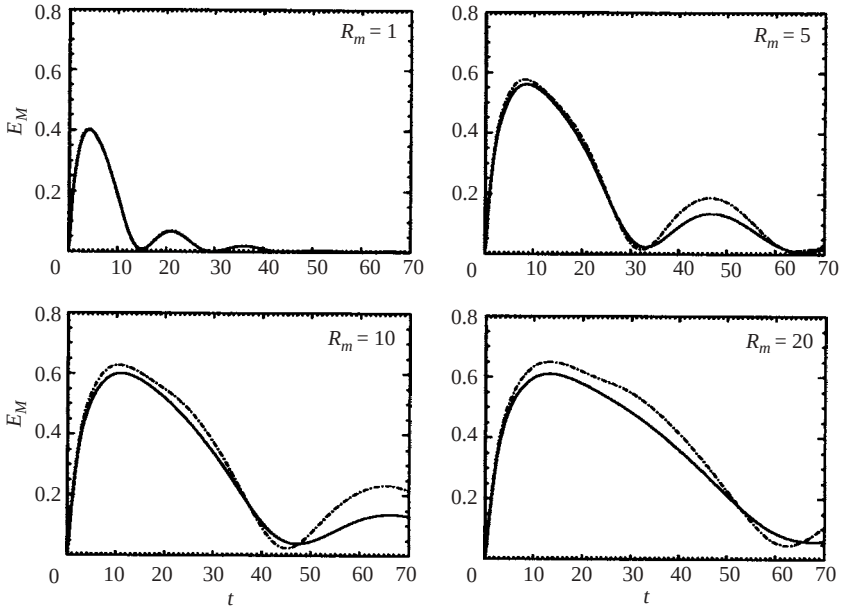

FIGURE 10. As for figure 9, but $N = 10$.

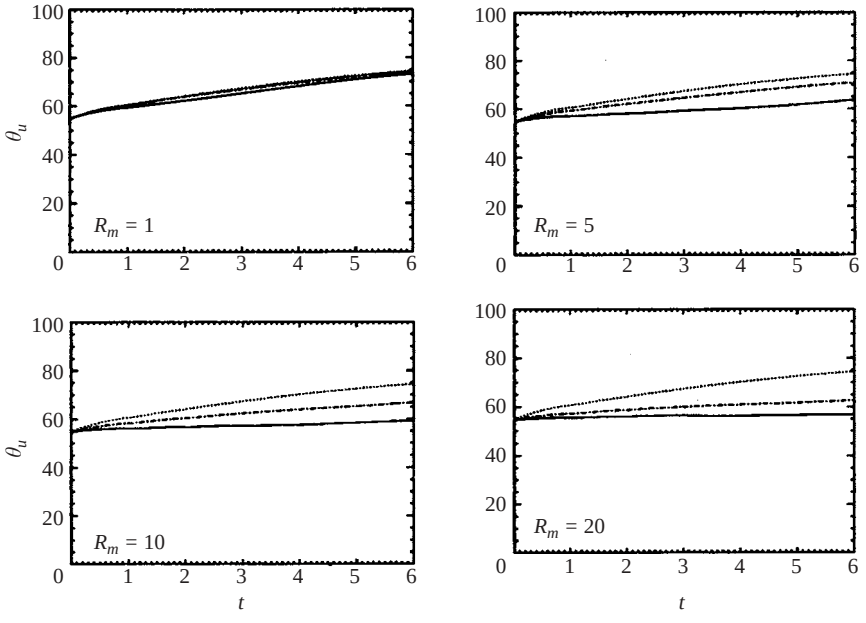

FIGURE 11. Evolution with time of the anisotropy angle θ_u ($N = 1$). ———, MHD; – · –, QL approximation; ·····, QS approximation.

4.2.3. *Anisotropy*

In figures 11 and 12, the anisotropy angle θ_u computed from the QL approximation and MHD is displayed. For reference, we have also included the anisotropy evolutions predicted using the QS approximation, which, as expected, are inadequate, especially for $R_m = 10$ and 20. In the runs with $N = 1$, the anisotropy predicted by the QL

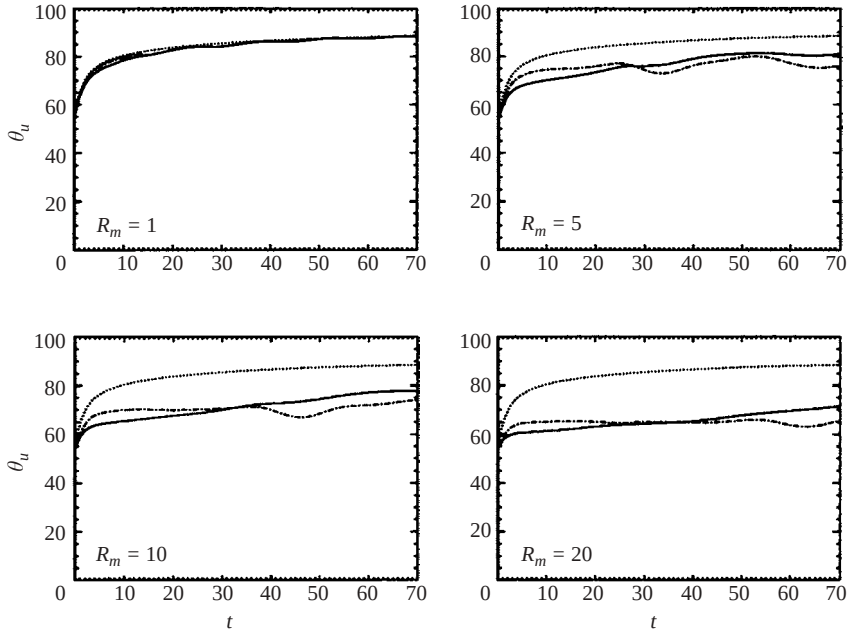

FIGURE 12. As for figure 11, but $N = 10$.

approximation is always more pronounced than for MHD. For the runs at $N = 10$, the same remark holds for the beginning of the decay. After a certain time, the trend inverses and the anisotropy is more pronounced in the case of MHD. This appears to be due to a rapid saturation of anisotropy in the QL runs.

The comparison of the anisotropy angles θ_b are presented in figures 13 and 14. Here, the trend is given by an underestimate of θ_b by the QL approximation. The discrepancy is somewhat more important for the runs where $N = 1$.

The initial trends observed for both θ_u and θ_b are to be expected. Indeed, it is clear that the additional nonlinear terms present in the MHD equations tend to restore isotropy. This effect will be more pronounced at the beginning of the decay when the flow is more turbulent. In the case of θ_u, it is therefore natural to observe an initial overestimate of θ_u by the QL approximation. Similarly, we know from MHD results discussed earlier that θ_b starts from an initial value of $\simeq 39.2^\circ$ and evolves progressively towards values close to the isotropic value of 54.7°. This trend should be slower in the QL case because of the absence of the nonlinear terms and this is exactly what is observed in figures 13 and 14.

4.2.4. *One-point turbulence structure tensors*

The anisotropy angles θ_u and θ_b provide a scalar measure of anisotropy. For the purpose of modelling MHD flows, especially flows with mean deformation, it is also important to have a directional (tensorial) one-point description of anisotropy. A one-point statistical measure of anisotropy for the hydrodynamic field is possible in terms of the *structure anisotropy tensors*, introduced by Kassinos, Reynolds and Rogers (2001) and Reynolds & Kassinos (1995). (For possible connections between the turbulence structure tensors and the MHD correlation tensors see Oughton, Rädler & Matthaeus (1997).) Formally, these tensors are defined using the vector

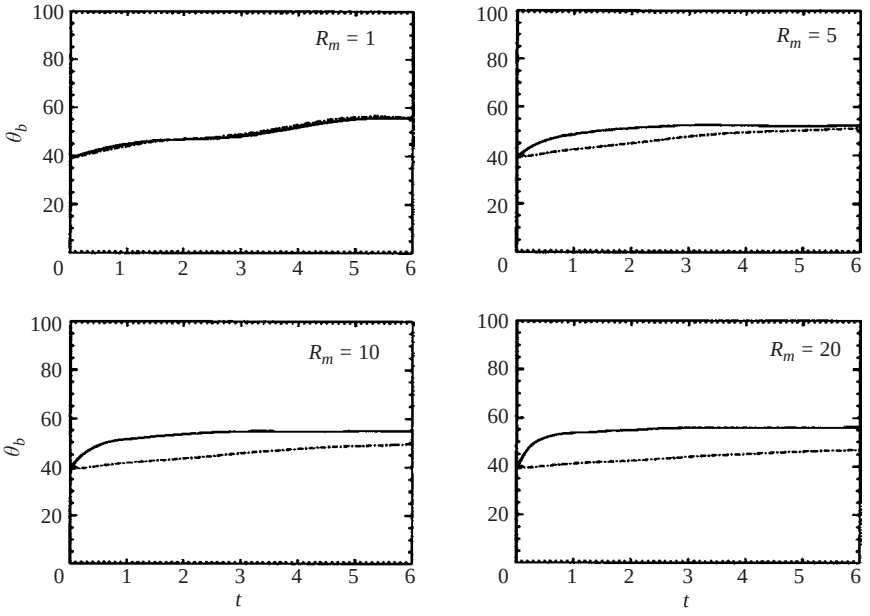

FIGURE 13. Evolution with time of the anisotropy angle θ_b ($N = 1$). ———, MHD; – · –, QL approximation.

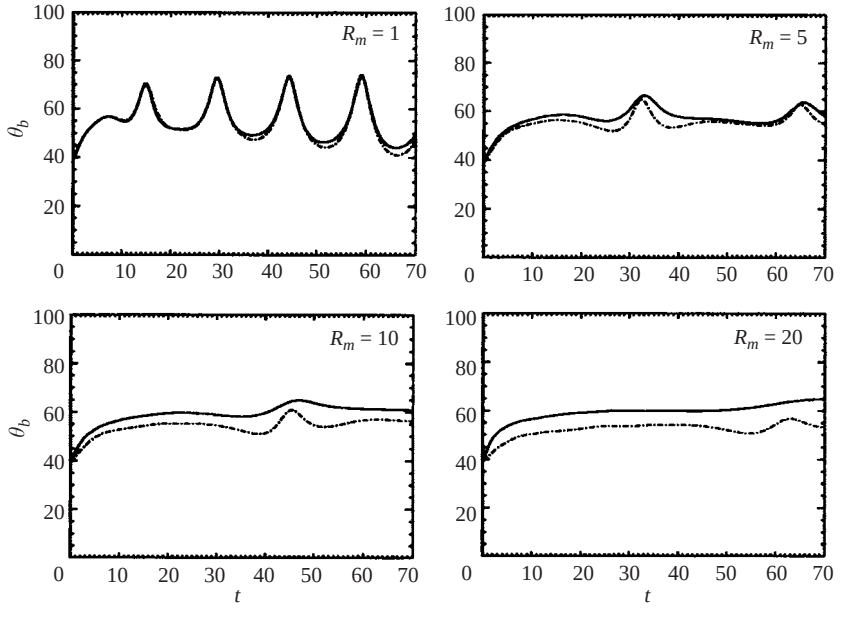

FIGURE 14. As for figure 13, but $N = 10$.

streamfunction Ψ_i of the turbulence, which in turn is defined by

$$u_i' = \epsilon_{ijk}\Psi_{k,j}', \qquad \Psi_{i,kk}' = -\omega_i', \qquad \Psi_{k,k}' = 0. \tag{4.5}$$

In the above relations, the superscript $'$ is used to specify the fluctuating parts of each variable used. Furthermore, ω_i' is the fluctuation of the vorticity of the flow:

$\omega' = \nabla \times \boldsymbol{u}'$. Note also that Ψ' is a local quantity that contains non-local turbulence information.

Here, we make use of simpler definitions that are valid for homogeneous turbulence. The Reynolds stress tensor can be expressed as

$$R_{ij} = \int E_{ij}(\boldsymbol{k})\, \mathrm{d}^3\boldsymbol{k}, \tag{4.6}$$

where $E_{ij}(\boldsymbol{k}) \sim \overline{\hat{u}_i(\boldsymbol{k})\hat{u}_j^*(\boldsymbol{k})}$ is the velocity spectrum tensor, $\boldsymbol{k}$ is the wavenumber vector, hats denote Fourier coefficients and $*$ denotes a complex conjugate. (In homogeneous fields, discrete Fourier expansions can be used to represent individual realizations in a box of length L; then the discrete cospectrum of two fields $\boldsymbol{f}$ and $\boldsymbol{g}$ is given by $\tilde{X}_{ij}(\boldsymbol{k}) = (L/2\pi)^3 \overline{\hat{f}_i(\boldsymbol{k})\hat{g}_j^*(\boldsymbol{k})}$, where the bar represents an ensemble average over the box. The cospectrum of two fields $X_{ij}(\boldsymbol{k})$ is the limit of the discrete cospectrum $\tilde{X}_{ij}$ as $L \to \infty$. Here we use $X_{ij}(\boldsymbol{k}) \sim \overline{\hat{f}_i(\boldsymbol{k})\hat{g}_j^*(\boldsymbol{k})}$ as a shorthand notation, but the exact definition should be kept in mind.) Note that if $u_1' = 0$ everywhere, then $R_{11} = 0$. We have emphasized (Kassinos & Reynolds 1994; Kassinos *et al.* 2001) that R_{ij} describes the *componentality* of the turbulence, but not its *dimensionality*. Two-dimensional turbulence need not be two-component; it could be one-, two-, or three-component.

The structure dimensionality tensor is

$$D_{ij} = \int \frac{k_i k_j}{k^2} E_{nn}(\boldsymbol{k})\, \mathrm{d}^3\boldsymbol{k}. \tag{4.7}$$

Like R_{ij}, D_{ij} is dominated by the large-scale energy-containing turbulence. We see that D_{ij} is determined by the energy distribution along rays in $\boldsymbol{k}$-space. If the turbulence is independent of x_1 then $D_{11} = 0$, since there is no energy associated with modes having a non-zero k_1 component of the wavenumber vector.

The circulicity tensor is

$$F_{ij} = \int \frac{1}{k^2} W_{ij}(\boldsymbol{k})\, \mathrm{d}^3\boldsymbol{k}. \tag{4.8}$$

where $W_{ij}(\boldsymbol{k})$ is the (fluctuating) vorticity spectrum tensor. Hence, F_{ij} is determined by the vorticity of the large-scale energy-containing turbulence. If the large-scale vorticity is aligned with the x_1-axis, then $F_{ij} = 0$ except for F_{11}. F_{ij} provides information on the large-scale circulation of the turbulence.

For homogeneous turbulence, the traces of all three tensors are equal to twice the kinetic energy:

$$R_{ii} = D_{ii} = F_{ii} = q^2 = 2E_k. \tag{4.9}$$

Moreover, for homogeneous turbulence these tensors are not linearly independent; they satisfy a constitutive relationship:

$$R_{ij} + D_{ij} + F_{ij} = q^2\delta_{ij}. \tag{4.10}$$

It is convenient to normalize each of these tensors by their trace:

$$r_{ij} = R_{ij}/R_{kk}, \qquad d_{ij} = D_{ij}/D_{kk}, \qquad f_{ij} = F_{ij}/F_{kk}. \tag{4.11}$$

Of course, $r_{ii} = d_{ii} = f_{ii} = 1$ and any particular component of the normalized tensors can vary only between 0 and 1. For isotropic turbulence,

$$r_{ij} = d_{ij} = f_{ij} = \tfrac{1}{3}\delta_{ij}\,. \tag{4.12}$$

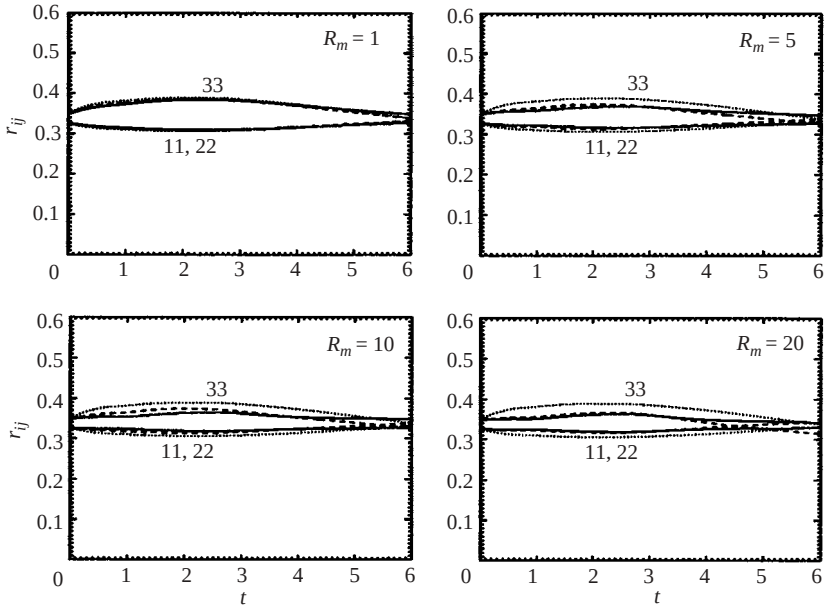

FIGURE 15. ———, MHD; – – –, QL approximation; ·····, QS approximation ($N = 1$). In each plot, the label '33' designates the $i = 3$, $j = 3$ component of the respective diagnostics while the label '11,22' designates the average between the components $i = 1$, $j = 1$ and $i = 2$, $j = 2$ of the respective diagnostics, e.g. $(r_{11} + r_{22})/2$.

Anisotropy invariant maps, such as the one introduced by Lumley (1978) for the Reynolds stress, can be formed for each of the structure anisotropy tensors (for examples see Kassinos & Reynolds 1994).

The evolution of the componentality and dimensionality tensors is shown in figures 15–18. The general trends are consistent with the picture of anisotropy obtained from θ_u and θ_b. For example, anisotropy is more pronounced at $N = 10$ than at $N = 1$, while at a given N, anisotropy becomes progressively suppressed as R_m is increased and nonlinear effects become important. The QS approximation (which implicitly assumes $R_m \to 0$) is of course not able to capture this trend, and the quality of its predictions is unsatisfactory especially for $R_m = 10$ and $R_m = 20$. It is therefore important that the QL approximation captures enough of the nonlinear effects to be able to adequately represent this trend for the range of R_m values that we have tested.

The levels of componentality anisotropy (see figures 15 and 16) predicted by the QL approximation are in excellent agreement with those produced by the MHD runs. Perhaps the fact that nonlinear terms are retained in the momentum equation contributes to this excellent agreement. Also, it was shown in Moffatt (1967) that in the final stages of decay, we should have $r_{33} \approx r_{11} + r_{22}$ when viscous effects are neglected in the limit $R_m \to 0$. From figures 15 and 16 (see dotted lines), it is clear that this result is not valid here and thus that molecular viscosity cannot be neglected compared to Joule dissipation.

As shown in figures 17 and 18, the overall agreement between the dimensionality anisotropy levels predicted by the QL approximation and those obtained via MHD is satisfactory but not perfect. The QL approximation consistently overpredicts the dimensionality anisotropy at $N = 1$, whereas this trend is reversed at $N = 10$, where, at least at larger times, MHD seems to predict higher anisotropy levels for the

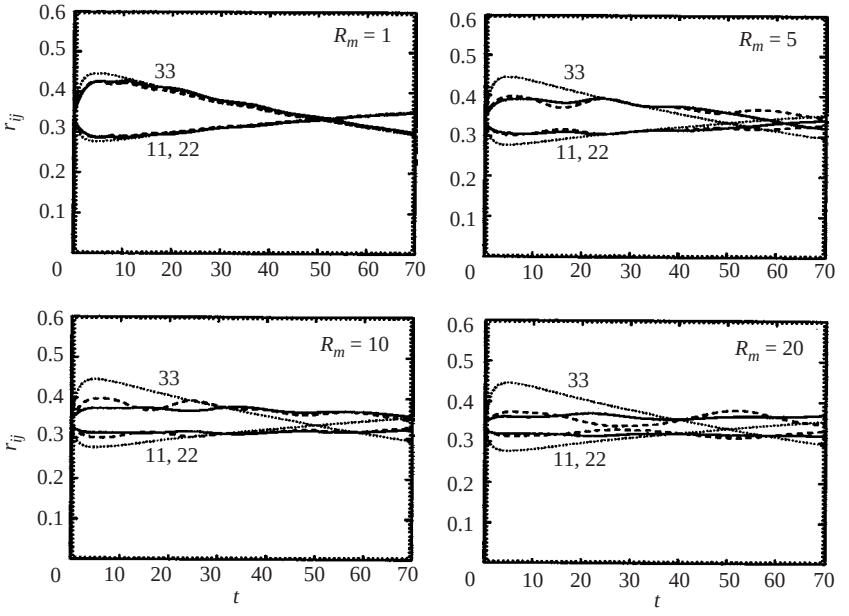

FIGURE 16. As figure 15, but $N = 10$.

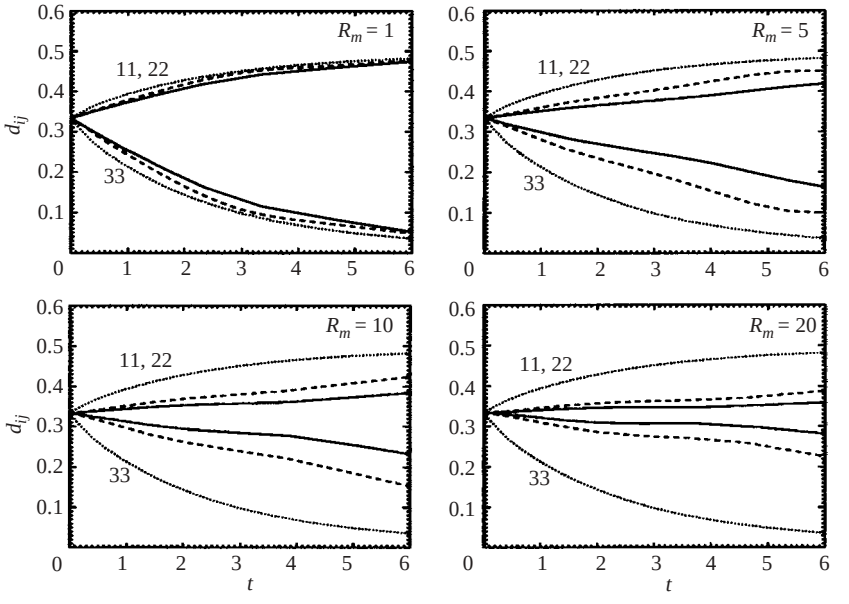

FIGURE 17. As figure 15, but for the dimensionality tensors.

dimensionality. However, the QL approximation exhibits the correct trends as R_m is varied and provides a systematic improvement over the QS approximation for all the runs performed.

Overall, the structure anisotropy tensors confirm the traditional picture of elongation of the energy-containing structures in the direction x_3 of external mean magnetic field. This elongation is evidenced by the fact that d_{33} is suppressed relative

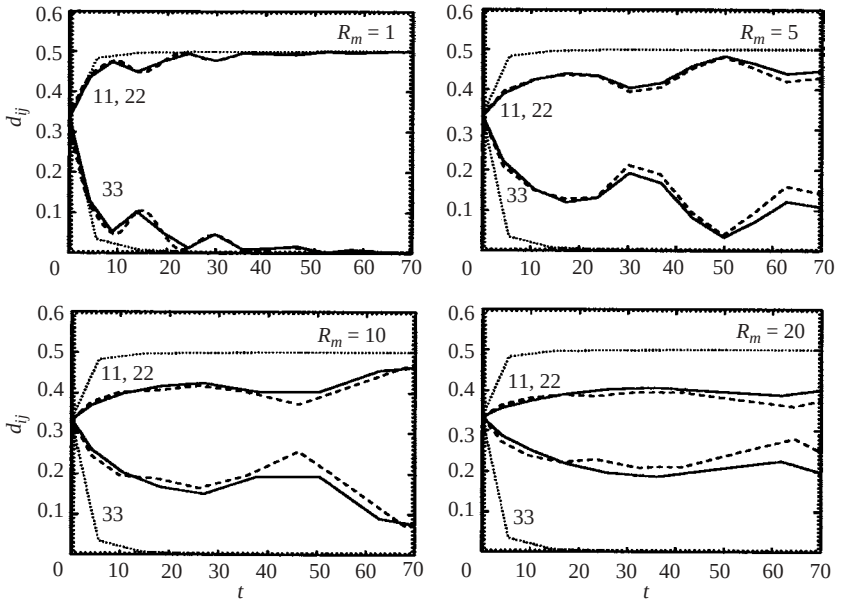

FIGURE 18. As figure 17, but $N = 10$.

to d_{11} and d_{22}, and it is more pronounced in the case $N = 10$. The turbulence tends to become two-dimensional; note, however, that it remains three-component (none of the r_{ij} components is appreciably suppressed).

5. Conclusions and future plans

The quasi-static (QS) approximation offers a valuable engineering approximation for the prediction of MHD flows at small magnetic Reynolds numbers $R_m \ll 1$. However, important technological applications, such as advanced propulsion and flow control schemes for hypersonic vehicles, involve MHD and MGD flows at moderate magnetic Reynolds numbers $1 \lesssim R_m \lesssim 20$. In order to devise successful schemes for the prediction of these technological flows we need to understand better the intermediate regime that bridges the domain where the QS approximation is valid and the high-R_m regime, where full nonlinear MHD is the only resort.

By studying the case of decaying homogeneous MHD turbulence, we have established that the quasi-static (QS) approximation is valid for $R_m \lesssim 1$, but progressively deteriorates as R_m is increased beyond 1. The magnetic Stuart number does not seem to have a strong effect on the accuracy of the QS approximation. That is, at a given R_m, the accuracy of the QS approximation is roughly the same for $N = 1$ as it is for $N = 10$.

We have studied another approximation, the QL approximation, for use at higher R_m. As with the QS approximation, this approximation assumes small magnetic fluctuations, but it resolves the time dependence of these fluctuations explicitly. The QL approximation performs like the QS approximation for $R_m \lesssim 1$, but has the advantage that it retains good agreement with MHD for $1 \lesssim R_m \lesssim 20$. It should be noted that $R_m = 20$ is the highest value of the magnetic Reynolds number that we have tested during this effort. Therefore, our numerical simulations indicate that the QL approximation should be adopted in place of the QS approximation for flows with a

moderate value of the magnetic Reynolds number ($1 \lesssim R_m \lesssim 20$). At higher values of the magnetic Reynolds number, we cannot avoid using the full MHD equations (at least for the type of flow considered here). Numerical tests performed at $R_m = 50$ and $R_m = 100$ (not reported in the article) show that the QL approximation is inadequate in that regime. Thus, the QL approximation cannot be applied directly to study the dynamo problem.

In terms of computational costs, the QS approximation is clearly the cheapest of the three methods used during our study. It has fewer nonlinear terms to evaluate, and the time step required to advance the flow is governed by the time scale of the velocity field which, for most industrial cases involving liquid metal, is significantly longer than the time scale of the underlying magnetic field. There is no doubt that the QS approximation should be the approximation of choice for the prediction of flows with $R_m \ll 1$.

The computational cost of solving directly the QL approximation transport equations does not depart enormously from that of solving the MHD equations, but nevertheless allows a reasonable gain since fewer nonlinear terms need be evaluated. The appeal of the QL approximation lies more in the prospect of simpler turbulence models for conductive flows at moderate magnetic Reynolds number. Indeed, the structure of (4.1) and (4.2) is simpler than that of the MHD equations. The gain in simplicity is even more substantial in terms of the Reynolds-averaged equations. We thus have a strong hope that devising turbulence models in the framework of the QL approximation should be an easier task than trying to tackle the MHD equations. In fact, we are currently engaged in the development of structure-based closures of the QL approximation for homogeneous turbulence in a conductive fluid subject to mean deformation and a uniform external magnetic field. This effort builds on earlier work that dealt with the modelling of decaying homogeneous MHD turbulence.

The authors are grateful to the Center for Turbulence Research for hosting and providing financial support for part of this work during the 2002 Summer Program. S. K. wishes to acknowledge partial support of this work by AFOSR. B. K. and D. C. are researchers of the Fonds National pour la Recherche Scientifique (Belgium). This work has also been supported in part by the Communauté Française de Belgique (ARC 02/07-283) and by the contract of association EURATOM – Belgian state. The content of the publication is the sole responsibility of the authors and it does not necessarily represent the views of the Commission or its services.

REFERENCES

Davidson, P. 2001 *An Introduction to Magnetohydrodynamics*. Cambridge University Press.

Davidson, P. A. 1995 Magnetic damping of jets and vortices. *J. Fluid Mech.* **299**, 153–186.

Hossain, M. 1991 Inverse energy cascades in three dimensional turbulence. *Phys. Fluids* B **3**, 511–514.

Kassinos, S. C. & Reynolds, W. C. 1994 A structure-based model for the rapid distortion of homogeneous turbulence. *Tech. Rep.* TF-61. Mechanical Engineering Dept.

Kassinos, S. C. & Reynolds, W. C. 1999 Structure-based modeling for homogeneous MHD turbulence. In *Annual Research Briefs 1999*, pp. 301–315. Stanford University and NASA Ames Research Center: Center for Turbulence Research.

Kassinos, S. C., Reynolds, W. C. & Rogers, M. M. 2001 One-point turbulence structure tensors. *J. Fluid Mech.* **428**, 213–248.

Lehnert, B. 1955 The decay of magneto-turbulence in the presence of a magnetic field and Coriolis force. *Q. Appl. Maths* **12**, 321–341.

Lumley, J. L. 1978 Computational modeling of turbulent flows. *Adv. Appl. Mech.* **18**, 123.

Moffatt, H. K. 1967 On the suppression of turbulence by a uniform magnetic field. *J. Fluid Mech.* **28**, 571–592.

Oughton, S., Priest, E. & Matthaeus, W. 1994 The influence of a mean magnetic field on three-dimensional magnetohydrodynamic turbulence. *J. Fluid Mech.* **280**, 95.

Oughton, S., Rädler, K.-H. & Matthaeus, W. 1997 General second-rank correlation tensors for homogeneous magnetohydrodynamic turbulence. *Phys. Rev.* E **56**, 2875.

Poggie, J. & Gaitonde, D. V. 2002 Magnetic control of flow past a blunt body: numerical validation and exploration. *Phys. Fluids* **14**, 1720.

Reynolds, W. C. & Kassinos, S. C. 1995 One-point turbulence structure tensors. *Proc. R. Soc. Lond.* A **451**, 87–104.

Roberts, P. H. 1967 *An Introduction to Magnetohydrodynamics*. American Elsevier, New York.

Schumann, U. 1976 Numerical simulation of the transition from three- to two-dimensional turbulence under a uniform magnetic field. *J. Fluid Mech.* **74**, 31–58.

Shebalin, J. V., Matthaeus, W. H. & Montgomery, D. 1983 Anisotropy in MHD turbulence due to a mean magnetic field. *J. Plasma Phys.* **29**, 525–547.

Sommeria, J. & Moreau, R. 1982 Why, how, and when, MHD turbulence becomes two-dimensional. *J. Fluid Mech.* **118**, 507–518.

Zikanov, O. & Thess, A. 1998 Direct numerical simulation of forced mhd turbulence at low magnetic Reynolds number. *J. Fluid Mech.* **358**, 299–233.